

Fabric dependence of bone ultrasound

STEPHEN C. COWIN*, LUIS CARDOSO

The New York Center for Biomedical Engineering, The Departments of Biomedical & Mechanical Engineering, The School of Engineering of The City College, and The Graduate School of The City University of New York.

Current diagnosis of bone loss and osteoporosis is based on the measurement of the Bone Mineral Density (BMD) or the apparent mass density. Unfortunately, in most clinical ultrasound densitometers: 1) measurements are often performed in a single anatomical direction, 2) only the first wave arriving to the ultrasound probe is characterized, and 3) the analysis of bone status is based on empirical relationships between measurable quantities such as Speed of Sound (SOS) and Broadband Ultrasound Attenuation (BUA) and the density of the porous medium. However, the existence of a second wave in cancellous bone has been reported, which is an unequivocal signature of poroelastic media, as predicted by Biot's poroelastic wave propagation theory. A fabric-dependent anisotropic poroelastic approach is employed as a theoretical framework to describe the microarchitectural-dependent relationship between measurable wave properties and the elastic constants of trabecular bone, and thus represents an alternative for bone quality assessment beyond BMD alone.

Key words: poroelasticity, fabric, anisotropy, compressibility, wave propagation, bone

1. Introduction

The current standard for the diagnosis of bone loss and osteoporosis consists in determining the amount of Bone Mineral Density (BMD) measured with a Dual Energy X-ray Absorptiometry (DEXA) system. The BMD is highly correlated to bone mass when measured in the spine, wrist and femoral neck. However, a significant number of women diagnosed with osteoporosis based on BMD measurement do not suffer fractures, whereas many women with normal BMD do [1]. These studies have demonstrated that BMD measurements lack both sensitivity and selectivity to effectively identify patients with decreased bone strength and at risk of fracture, indicating that other factors besides bone mass play an important role in osteoporosis.

Ultrasound wave propagation is an attractive alternative to diagnose osteoporosis [2]–[4] because it is non-ionizing, inexpensive and non-invasive. More

importantly, ultrasound waves are elastic vibrations that can provide direct information on the mechanical properties of the medium in which they propagate. Clinical ultrasound in bone is based on a wave transmission technique to measure the Speed of Sound (SOS) and Broadband Ultrasound Attenuation (BUA) in the heel bone (calcaneum). Unfortunately, a major limitation associated with current clinical ultrasound systems [5] – often called ultrasound densitometers – consists in determining bone mass density as DEXA does, without taking advantage of the fact that ultrasound is sensitive to microarchitecture and tissue composition [6]–[8].

In most clinical ultrasound densitometer systems, only the first wave arriving to the ultrasound probe is identified. If only one wave is measured, the analysis is limited to an “equivalent medium approach” in which the solid trabecular structure cannot be distinguished from the fluid within the pores. However, the existence of a second wave in cancellous bone has been reported [9]–[12], which is an unequivocal sig-

* Corresponding author: Stephen C. Cowin, The New York Center for Biomedical Engineering, The Departments of Biomedical & Mechanical Engineering, The School of Engineering of The City College, and The Graduate School of The City University of New York, New York, NY 10031. Phone (212) 650-5208, e-mail: scowin@earthlink.net

Received: May 30th, 2010

Accepted for publication: June 10th, 2010

nature of poroelastic media. These two waves propagate with different velocities and have been shown to correspond to the fast and slow waves predicted by Biot's [13]–[18] poroelastic wave propagation theory. Therefore, a poroelastic wave propagation theory is conceptually more appropriate than an equivalent media approach to characterize the properties of the porous medium.

The application of poroelasticity to bone tissue [19] and geological materials [13]–[18], [20] has been described in the past, and a number of models based on the isotropic Biot theory of wave propagation in porous media have been used [9], [10], [21], [22] to explain acoustic wave propagation measurements on cancellous bone. However, isotropic poroelastic models cannot explain the variability of measured wave velocities [12] when bone becomes anisotropic as a consequence of age and osteoporosis. Bone porosity alone is an inappropriate parameter of cancellous bone acoustic properties when the medium is anisotropic. This is because a scalar – such as porosity or any densitometry measurement – does not have the capacity to fully describe the cancellous bone architecture: a tensorial quantity such as the fabric tensor is required.

Unfortunately, most clinical ultrasound densitometers depend on empirical relationships between SOS/BUA and bone density that have failed to improve the assessment of bone loss as provided by DEXA measurements. Furthermore, measurements of SOS and BUA are performed in a single direction at the calcaneum. Such measurement cannot fully describe the properties of anisotropic bone, for which multidirectional ultrasound measurements are required. In contrast, the fabric-dependent anisotropic poroelastic approach proposed in this study has the advantage of providing a theoretical framework to describe the relationship between measurable wave properties (SOS, BUA, etc) and the elastic constants of the trabecular bone structure. Since this poroelastic wave propagation theory depends on anisotropy and tissue composition in addition to bone mass density, it represents an alternative for bone quality assessment beyond BMD.

In this paper, the governing equations for wave motion in the linear theory of anisotropic poroelastic materials including the dependence of the constitutive relations upon fabric [1] are employed. Fabric is a quantitative stereological measure of the degree of structural anisotropy in the pore architecture of a porous medium (see [1] for references). With the exception of the addition of the fabric variable, a tensor, the formulation of wave motions in the context of poroelastic theory is consistent with classic and contempo-

rary literature in the field [13]–[18], [20]. Unchanged by the addition of anisotropy is the fact that the total elastic volumetric response in poroelasticity is due to a combination of the elastic volumetric response of the matrix material of the porous solid, the volumetric elastic response of the pore fluid, and the pore volume changes in the porous medium. The theory of wave propagation in fluid-saturated porous materials employing the fabric variable is summarized in section 2. The propagation conditions for plane waves in an anisotropic, fabric dependent, saturated porous medium are then derived in section 3, and the specialization of these results to the propagation in a principal direction of fabric are presented in section 4. The final section contains our discussion and concluding remarks.

2. Wave propagation in anisotropic porous media

In the papers of 1956 on wave propagation by BIOT [15], [16], \mathbf{u} represents the displacement vector of the solid matrix phase and \mathbf{U} represents the displacement vector of the fluid phase. These were the two basic kinematic quantities employed in those works. In [17], the displacement vector \mathbf{U} of the fluid phase was replaced by the displacement vector \mathbf{w} of the fluid relative to the solid, thus

$$\mathbf{w} = \mathbf{U} - \mathbf{u}. \quad (1)$$

The present development follows [17], [18] and the two basic kinematic fields are considered to be the displacement vectors \mathbf{u} and \mathbf{w} . The relative velocity of the fluid and solid components is, from (1), as follows

$$\dot{\mathbf{w}} = \dot{\mathbf{U}} - \dot{\mathbf{u}}. \quad (2)$$

The variation in fluid content ζ is defined as

$$\zeta = -\nabla \cdot \mathbf{w}. \quad (3)$$

The variation in fluid content ζ is the variation of the fluid volume per initial unit volume of the porous material due to diffusive fluid mass transport; it is defined as the difference between the volumetric strain of the pore space and the volumetric strain of the fluid volume in the pore space and is dimensionless.

The field equations of motion are [17], [1]

$$A_{ijkm} \frac{\partial^2 \mathbf{u}_k}{\partial x_m \partial x_j} + M_{ij} \frac{\partial^2 \mathbf{w}_k}{\partial x_k \partial x_j} = \rho \ddot{\mathbf{u}}_i + \rho_f \ddot{\mathbf{w}}_i, \quad (4)$$

$$M_{km} \frac{\partial^2 u_k}{\partial x_m \partial x_i} + M \frac{\partial^2 w_k}{\partial x_k \partial x_i} = \rho_f (\ddot{u}_i + J_{ij} \ddot{w}_j + \mu R_{ij} \dot{w}_j), \quad (5)$$

$$v = \frac{\omega}{k_{\text{Re}} + i\alpha_{\text{Im}}}. \quad (7)$$

where:

A_{ijkl} is Biot's elasticity tensor,

M_{km} is the proportionality tensor between the strain tensor and the fluid pressure p ,

M is the proportionality factor between the variation in fluid content ζ and the stress tensor,

R_{km} is the flow-resistivity tensor,

J_{km} is the micro-macro velocity average tensor,

ρ is the bulk density,

ρ_s represents the density of the solid matrix material,

ρ_f represents the density of the pore fluid.

The micro-macro velocity average tensor J_{km} acts like a density distribution function that relates the relative micro-solid-fluid velocity to its bulk volume average $\dot{\mathbf{w}}$. It is interesting to note that Biot's elasticity tensor A_{ijkl} differs from the drained elasticity tensor by the term $MA_{ij}A_{km}$, which is the open product of the Biot effective stress coefficient tensor \mathbf{A} with itself [1].

Equations (4) and (5) are two coupled wave equations for the solid displacement field \mathbf{u} and the displacement field \mathbf{w} of the fluid relative to the solid.

The propagation of a plane wave is represented kinematically by a direction of propagation, denoted by \mathbf{n} , a unit normal to the wave front, and \mathbf{a} or \mathbf{b} , which are the directions of displacement for the wave fronts associated with \mathbf{u} and \mathbf{w} , respectively. These two plane waves are represented by

$$\begin{aligned} \mathbf{u}(\mathbf{x}, t) &= \mathbf{a} e^{i\omega \left(\frac{\mathbf{n} \cdot \mathbf{x}}{v} - t \right)} = \mathbf{a} e^{i((k+i\alpha)\mathbf{n} \cdot \mathbf{x} - \omega t)} \\ &= \mathbf{a} e^{-\alpha \mathbf{n} \cdot \mathbf{x}} e^{i(k\mathbf{n} \cdot \mathbf{x} - \omega t)}, \\ \mathbf{w}(\mathbf{x}, t) &= \mathbf{b} e^{i\omega \left(\frac{\mathbf{n} \cdot \mathbf{x}}{v} - t \right)} = \mathbf{b} e^{i((k+i\alpha)\mathbf{n} \cdot \mathbf{x} - \omega t)} \\ &= \mathbf{b} e^{-\alpha \mathbf{n} \cdot \mathbf{x}} e^{i(k\mathbf{n} \cdot \mathbf{x} - \omega t)}, \end{aligned} \quad (6)$$

where:

v is the wave phase velocity in the direction \mathbf{n} ,

\mathbf{x} is the position vector,

ω is the frequency,

t is the time.

The relationship between the phase velocity v and the frequency ω of attenuating waves is a complex quantity, here represented by $k_{\text{Re}} + i\alpha_{\text{Im}}$

The imaginary part α is related to the wave attenuation as a function of travelled distance ($e^{-\alpha \mathbf{n} \cdot \mathbf{x}}$) and the real part k describes the wave vector and points in the direction \mathbf{n} . A transverse wave is characterized by $\mathbf{a} \cdot \mathbf{n} = 0$, a longitudinal wave by $\mathbf{a} \cdot \mathbf{n} = 1$. Substituting the representations (7) for the plane waves into the field equations (5) and (6) one obtains equations that are in [17], [18] and many other places

$$(\mathbf{Q}_{ik} - \rho v^2 \delta_{ik}) a_k + (C_{ik} - \rho_f v^2 \delta_{ik}) b_k = 0, \quad (8)$$

$$(C_{ik} - \rho_f v^2 \delta_{ik}) a_k$$

$$+ \left(Mn_k n_i - \rho_f v^2 \left\{ J_{ik} + \frac{i\mu}{\omega} R_{ik} \right\} \right) b_k = 0, \quad (9)$$

where the following notation has been introduced:

$$\mathbf{Q}_{ik} = A_{ijkl} n_m n_j, \quad C_{ik} = M_{ij} n_j n_k, \quad (10)$$

\mathbf{Q} is the acoustical tensor from elastic wave propagation,

\mathbf{C} represents the interaction of the velocity fields \mathbf{u} and \mathbf{w} .

Rewritten in matrix notation equations (8) and (9) take the form

$$(\mathbf{Q} - \rho v^2 \mathbf{1}) \cdot \mathbf{a} + (C - \rho_f v^2 \mathbf{1}) \cdot \mathbf{b} = 0, \quad (11)$$

$$(C - \rho_f v^2 \mathbf{1}) \cdot \mathbf{a}$$

$$+ \left(M\mathbf{n} \otimes \mathbf{n} - \rho_f v^2 \left\{ \mathbf{J} + \frac{i\mu}{\omega} \mathbf{R} \right\} \right) \cdot \mathbf{b} = 0. \quad (12)$$

Equations (11) and (12) represent an eigenvalue problem, the squares of the wave speeds v^2 representing the eigenvalues and the vectors \mathbf{a} and \mathbf{b} representing the eigenvectors. Rewriting equations (11) and (12) as a 6 by 6 matrix formed from the four 3 by 3 matrices that appear in (11) and (12) and also representing the two 3D vectors \mathbf{a} and \mathbf{b} as one 6D vector, the following representation is obtained:

$$\begin{bmatrix} \mathbf{Q} - \rho v^2 \mathbf{1} & C - \rho_f v^2 \mathbf{1} \\ C^T - \rho_f v^2 \mathbf{1} & M\mathbf{n} \otimes \mathbf{n} - \rho_f v^2 \left\{ \mathbf{J} + \frac{i\mu}{\omega} \mathbf{R} \right\} \end{bmatrix} \begin{bmatrix} \mathbf{a} \\ \mathbf{b} \end{bmatrix} = 0. \quad (13)$$

Equation (13) is a generalization of the *Christoffel equation* [23], [24] in anisotropic elastic wave propagation to the poroelastic case, the poroelastic Christoffel equation is a possible name for this result. Since the

right-hand side of this linear system of equations is a zero 6D vector, it follows from Cramer's rule that, in order to avoid the trivial solution, it is necessary to set the determinant of the 6 by 6 matrix equal to zero, thus

$$\begin{vmatrix} \mathbf{Q} - \rho v^2 \mathbf{1} & \mathbf{C} - \rho_f v^2 \mathbf{1} \\ \mathbf{C}^T - \rho_f v^2 \mathbf{1} & M \mathbf{n} \otimes \mathbf{n} - \rho_f v^2 \left\{ \mathbf{J} + \frac{i\mu}{\omega} \mathbf{R} \right\} \end{vmatrix} = 0. \quad (14)$$

2.1. Fabric dependence of tensors \mathbf{Q} , \mathbf{C} , \mathbf{J} and \mathbf{R}

Formulas relating the acoustic tensor \mathbf{Q} , the flow resistivity tensor \mathbf{R} and the tensor \mathbf{C} , representing the interaction of the velocity fields \mathbf{u} and \mathbf{w} , to the fabric tensor \mathbf{F} were obtained in [1] and are summarized in this subsection.

The dependence of the elastic acoustic tensor \mathbf{Q} upon the fabric tensor \mathbf{F} is given by

$$\begin{aligned} \mathbf{Q} = & (c_1^{cd} + c_2^{cd} \text{tr}\{\mathbf{F} \cdot \mathbf{n} \otimes \mathbf{n}\} + c_3^{cd} \text{tr}\{\mathbf{F}^2 \cdot \mathbf{n} \otimes \mathbf{n}\}) \mathbf{1} \\ & + q_1 \mathbf{n} \otimes \mathbf{n} + c_2^{cd} \mathbf{F} + q_2 (\mathbf{F} \cdot \mathbf{n} \otimes \mathbf{n} + \mathbf{n} \otimes \mathbf{F} \cdot \mathbf{n}) \\ & + c_3^{cd} \mathbf{F}^2 + q_3 (\mathbf{F}^2 \cdot \mathbf{n} \otimes \mathbf{n} + \mathbf{n} \otimes \mathbf{F}^2 \cdot \mathbf{n}) + q_4 \mathbf{F} \cdot \mathbf{n} \otimes \mathbf{F} \cdot \mathbf{n} \\ & + q_5 (\mathbf{F} \cdot \mathbf{n} \otimes \mathbf{F}^2 \cdot \mathbf{n} + \mathbf{F}^2 \cdot \mathbf{n} \otimes \mathbf{F} \cdot \mathbf{n}) \\ & + q_6 \mathbf{F}^2 \cdot \mathbf{n} \otimes \mathbf{F}^2 \cdot \mathbf{n}. \end{aligned} \quad (15)$$

The six scalar quantities defined in (15) are scalar-valued functions of ϕ , II and III , ϕ is the porosity and II and III are the second and third invariants of the fabric tensor \mathbf{F} .

The formula for the tensor \mathbf{C} is

$$\begin{aligned} C_{ik} = & M n_i n_k \\ & - \frac{M}{3K^m} \{ a_0^{cd} n_i + a_1^{cd} F_{ij} n_j + a_{II}^{cd} F_{iq} F_{qj} n_j \} n_k. \end{aligned} \quad (16)$$

The micro-macro velocity average tensor \mathbf{J} is related to the fabric by

$$J_{ij} = j_1 \delta_{ij} + j_2 F_{ij} + j_3 F_{iq} F_{qj}, \quad (17)$$

where j_1 , j_2 , and j_3 are the functions of ϕ , II and III . Similarly, the flow-resistivity tensor \mathbf{R} is related to the fabric by

$$R_{ij} = r_1 \delta_{ij} + r_2 F_{ij} + r_3 F_{iq} F_{qj}, \quad (18)$$

where:

r_1 , r_2 , and r_3 are the functions of ϕ , II and III ,

\mathbf{R} is equivalent to the inverse of the second-rank intrinsic permeability tensor \mathbf{K} .

2.2. Tortuosity, fabric, frequency dependence

The relationship between the second-rank intrinsic permeability tensor \mathbf{K} and the fabric tensor \mathbf{F} is obtained by assuming that \mathbf{K} is an isotropic function of \mathbf{F} . The relationship between two second-rank symmetric tensors in which one is an isotropic function of the other then produces the relationship

$$K_{ij} = k_1 \delta_{ij} + k_2 F_{ij} + k_3 F_{iq} F_{qj}. \quad (19)$$

This permeability tensor can be rewritten using the intrinsic permeability κ_0 as

$$K_{ij} = K_1 \delta_{ij} + K_2 F_{ij} + K_3 F_{iq} F_{qj}, \quad (20)$$

where:

K_{ij} is the intrinsic permeability which is representative of the geometry of the porous medium only, not the fluid,

K_1 , K_2 , and K_3 are the functions of ϕ , II and III .

The hydraulic permeability K_{ij}/μ differs from the intrinsic permeability where μ is the pore fluid viscosity. We introduce the symbol κ_0 to represent the value of the intrinsic permeability tensor when it is averaged over all possible directions at a point

$$\kappa_0 = \frac{\pi^2}{2} (2K_1 + K_2 \text{tr} \mathbf{F} + K_3 \text{tr} [\mathbf{F} \cdot \mathbf{F}^T]), \quad (21)$$

and rewrite (63) as

$$K_{ij} = \kappa_0 (K_1^A \delta_{ij} + K_2^A F_{ij} + K_3^A F_{iq} F_{qj}), \quad (22)$$

where

$$K_i^A = \frac{K_i}{\kappa_0}, \quad i = 1, 2, 3. \quad (23)$$

The fabric tensor describes the configuration and orientation of the flow paths, and the average intrinsic permeability κ_0 is proportional to the squared average diameter of the pores d through which the fluid moves:

$$\kappa_0 \propto d^2. \quad (24)$$

The tensor \mathbf{K} takes into account dissipation phenomena due to viscous losses; however, expression (22) for permeability is adequate only for low frequencies of fluid motion and needs to be corrected to take into account the change in fluid flow regime occurring between low and high frequencies of wave propagation. This correction was originally introduced by JOHNSON [25] describing a dynamic permeability

in a porous medium system characterized by orthogonally intersected tubes.

$$K_{ij}(\omega) = \kappa_0 \left[1 - 2 \frac{J_1(d\chi)}{d\chi J_0(d\chi)} \right] \times (K_1 \delta_{ij} + K_2 F_{ij} + K_3 F_{iq} F_{qj}). \quad (25)$$

The dynamic permeability tensor \mathbf{K} is then described as a function of the average intrinsic permeability κ_0 , the fabric tensor and the Bessel functions that characterize the dynamics of the oscillatory fluid flow inside a cylindrical channel. In this equation, J_1 and J_0 are, respectively, the first order and zeroth order Bessel functions of the first kind; d corresponds to the average characteristic pore dimension; and the inverse of the viscous skin depth χ is defined as a function of the angular frequency ω , the fluid mass density ρ^f and the dynamic viscosity of the fluid μ :

$$\chi = \left(\frac{i\omega\rho^f}{\mu} \right)^{1/2}. \quad (26)$$

The motion of the viscous fluid relative to the solid is characterized by the velocity gradient profile perpendicular to the pore wall, as a consequence of the viscous properties of the fluid. If the characteristic thickness of the viscous layer (viscous skin depth) is greater than the pore diameter d , the resulting velocity profile will be parabolic throughout the pore lumen and the fluid flow will be the Poiseuille flow. However, as the frequency increases, the viscous skin depth becomes smaller than the pore radius, and the profile of the fluid flow is no longer parabolic. A consequence of this change in the fluid flow regime into the pore is the existence of a critical frequency $f_{\text{crit}} = \mu / \pi \rho^f d^2$, distinguishing the frequency regions where the slow wave may theoretically propagate. In the low frequency regime (below $\omega_{\text{crit}} = 2\pi f_{\text{crit}}$), the viscous coupling phenomenon dominates over the inertial one, locking together fluid and solid displacements, and thus hampering the genesis of the slow wave. However, at high frequencies, the viscous coupling phenomenon becomes much less important than the inertial one, and the relative movement between fluid and solid is no longer impeded. Above this critical frequency, both fast and slow waves may be expected to propagate.

The inverse of the second-rank intrinsic permeability tensor \mathbf{K} , the flow-resistivity tensor \mathbf{R} , is related to the fabric in the situation representing the frequency dependence by (18) where

$$r_i(\omega, \phi, II, III) = \frac{r_i^A(\phi, II, III)}{\kappa_0 \left[1 - 2 \frac{J_1(d\chi)}{d\chi J_0(d\chi)} \right]}, \quad (27)$$

$$R_{ij}(\omega) = \frac{1}{\kappa_0 \left[1 - 2 \frac{J_1(d\chi)}{d\chi J_0(d\chi)} \right]} \times (r_1 \delta_{ij} + r_2 F_{ij} + r_3 F_{iq} F_{qj}), \quad (28)$$

where the r_i^A , $i = 1, 2, 3$, are the functions of ϕ , II and III . Following [25] and [26] the tortuosity tensor $\mathbf{A}(\omega)$ is introduced

$$\rho_f \mathbf{A}(\omega) \cdot \frac{\partial \mathbf{v}}{\partial t} = -\nabla p, \quad \left(\rho_f A_{ij}(\omega) \frac{\partial v_j}{\partial t} = -\frac{\partial p}{\partial x_i} \right), \quad (29)$$

and using Darcy's law it follows that

$$\mathbf{A}(\omega) = \frac{i\mu\phi}{\omega\rho_0} \mathbf{K}^{-1}(\omega) = \frac{i\mu\phi}{\omega\rho_0} \mathbf{R}(\omega), \quad (30)$$

if we assume that $\mathbf{v} = \text{constant} \cdot e^{-i\omega t}$. From (18) and (28) it follows that

$$A_{ij}(\omega) = \frac{i\mu\phi}{\omega\rho_0} (r_1 \delta_{ij} + r_2 F_{ij} + r_3 F_{iq} F_{qj}), \quad (31)$$

establishing a connection between the tortuosity tensor and the fabric tensor in the case of harmonic wave propagation, where the r_i are given by (27). We have not explored this relationship yet, but we anticipate that this relationship will yield relationships between the tortuosity tensor and the curvature and torsion of the fluid channels in the porous material.

3. Propagation of waves along the principal axes of symmetry in orthotropic porous media

3.1. Phase velocity and phase direction

In this section, the solution is developed for waves that propagate in the direction of a principal axis of the fabric tensor. The direction of propagation is selected to be the one direction, thus \mathbf{F} and \mathbf{n} are given by

$$\mathbf{n} = \{1, 0, 0\} \quad \text{and} \quad \mathbf{F} = \begin{bmatrix} F_1 & 0 & 0 \\ 0 & F_2 & 0 \\ 0 & 0 & F_3 \end{bmatrix}, \quad (32)$$

and the displacement vectors reduce to

$$\begin{aligned} \mathbf{u}(\mathbf{x}, t) &= \mathbf{a}e^{i\omega\left(\frac{x_1}{v}-t\right)} = \mathbf{a}e^{i((k+i\alpha)x_1-\omega t)} = \mathbf{a}e^{-\alpha x_1}e^{i(kx_1-\omega t)}, \\ w(\mathbf{x}, t) &= \mathbf{b}e^{i\omega\left(\frac{x_1}{v}-t\right)} = \mathbf{b}e^{i((k+i\alpha)x_1-\omega t)} \\ &= \mathbf{b}e^{-\alpha x_1}e^{i(kx_1-\omega t)}. \end{aligned} \quad (33)$$

The solution to the problem is the solution of the 6 by 6 system of equations given by (13), thus the values of the tensors \mathbf{J} , \mathbf{R} , \mathbf{C} and \mathbf{Q} in the coordinate system of the principal axes of the fabric tensor and at the vector $\mathbf{n} = \{1, 0, 0\}$ are determined first. Under these conditions \mathbf{J} and \mathbf{R} are given by

$$\mathbf{J} = \begin{bmatrix} J_{11} & 0 & 0 \\ 0 & J_{22} & 0 \\ 0 & 0 & J_{33} \end{bmatrix}, \quad \mathbf{R} = \begin{bmatrix} R_{11} & 0 & 0 \\ 0 & R_{22} & 0 \\ 0 & 0 & R_{33} \end{bmatrix}, \quad (34)$$

where \mathbf{R} and \mathbf{J} are given by (17) and (18), thus

$$\mathbf{J} = \begin{bmatrix} j_1 + j_2 F_1 + j_3 F_1^2 & 0 & 0 \\ 0 & j_1 + j_2 F_2 + j_3 F_2^2 & 0 \\ 0 & 0 & j_1 + j_2 F_3 + j_3 F_3^2 \end{bmatrix}, \quad (35)$$

$\mathbf{R} =$

$$\begin{bmatrix} R_1 + R_2 F_1 + R_3 F_1^2 & 0 & 0 \\ 0 & R_1 + R_2 F_2 + R_3 F_2^2 & 0 \\ 0 & 0 & R_1 + R_2 F_3 + R_3 F_3^2 \end{bmatrix}, \quad (36)$$

\mathbf{C} is given by (16) as

$$\begin{aligned} C_{ik} &= Mn_i n_k - \frac{M}{3K^m} \\ &\times \{a_0^{cd} n_i + a_I^{cd} F_{ij} n_j + a_{II}^{cd} F_{iq} F_{qj} n_j\} n_k, \end{aligned} \quad (37)$$

$$\mathbf{C} = \begin{bmatrix} C_{11} & 0 & 0 \\ 0 & 0 & 0 \\ 0 & 0 & 0 \end{bmatrix},$$

and \mathbf{Q} is given by (15) as

$$\begin{aligned} \mathbf{Q} &= (c_1^{cd} + c_2^{cd} F_1 + c_3^{cd} F_1^2) \begin{bmatrix} 1 & 0 & 0 \\ 0 & 1 & 0 \\ 0 & 0 & 1 \end{bmatrix} \\ &+ q_1 \begin{bmatrix} 1 & 0 & 0 \\ 0 & 0 & 0 \\ 0 & 0 & 0 \end{bmatrix} + c_2^{cd} \begin{bmatrix} F_1 & 0 & 0 \\ 0 & F_2 & 0 \\ 0 & 0 & F_3 \end{bmatrix} \\ &+ q_2 \begin{bmatrix} 2F_1 & 0 & 0 \\ 0 & 0 & 0 \\ 0 & 0 & 0 \end{bmatrix} + c_3^{cd} \begin{bmatrix} F_1^2 & 0 & 0 \\ 0 & F_2^2 & 0 \\ 0 & 0 & F_3^2 \end{bmatrix} \\ &+ q_3 \begin{bmatrix} 2F_1^2 & 0 & 0 \\ 0 & 0 & 0 \\ 0 & 0 & 0 \end{bmatrix} + q_4 \begin{bmatrix} F_1^2 & 0 & 0 \\ 0 & 0 & 0 \\ 0 & 0 & 0 \end{bmatrix} \\ &+ 2q_5 \begin{bmatrix} IF_1^2 - IIF_1 + III & 0 & 0 \\ 0 & 0 & 0 \\ 0 & 0 & 0 \end{bmatrix} \\ &+ q_6 \begin{bmatrix} (I \bullet I - II)F_1^2 - (I \bullet II - III)F_1 + I \bullet III & 0 & 0 \\ 0 & 0 & 0 \\ 0 & 0 & 0 \end{bmatrix} \\ &= \begin{bmatrix} Q_{11} & 0 & 0 \\ 0 & Q_{22} & 0 \\ 0 & 0 & Q_{33} \end{bmatrix}, \end{aligned} \quad (38)$$

where

$$\begin{aligned} Q_{11} &= q_0^{11} + q_1^{11} F_1 + q_2^{11} F_1^2, \\ Q_{22} &= c_1^{cd} + c_2^{cd} (F_2 + F_1) + c_3^{cd} (F_2^2 + F_1^2), \\ Q_{33} &= c_1^{cd} + c_2^{cd} (F_3 + F_1) + c_3^{cd} (F_3^2 + F_1^2), \end{aligned} \quad (39)$$

and where

$$\begin{aligned} q_0^{11} &= c_1^{cd} + q_1 2IIIq_5 + q_6 I \bullet III, \\ q_2^{11} &= 2c_2^{cd} + 2q_2 - 2IIq_5 - q_6 (I \bullet II - III), \\ q_2^{11} &= 2c_3^{cd} + 2q_3 + q_4 + 2Iq_5 + (I \bullet I - II)q_6. \end{aligned} \quad (40)$$

In the coordinate system of the principal axes of the fabric tensor and at the vector $\mathbf{n} = \{1, 0, 0\}$, the four 3 by 3 sub-matrices that form the 6 by 6 matrix in equation (13) are given by

$$\mathbf{Q} - \rho v^2 \mathbf{1} = \begin{bmatrix} Q_{11} - \rho v^2 & 0 & 0 \\ 0 & Q_{22} - \rho v^2 & 0 \\ 0 & 0 & Q_{33} - \rho v^2 \end{bmatrix}, \quad (41)$$

$$\mathbf{C} - \rho_f v^2 \mathbf{1} = \mathbf{C}^T - \rho_f v^2 \mathbf{1} = \begin{bmatrix} C_{11} - \rho_f v^2 & 0 & 0 \\ 0 & -\rho_f v^2 & 0 \\ 0 & 0 & -\rho_f v^2 \end{bmatrix}, \quad (42)$$

$$M \mathbf{n} \otimes \mathbf{n} - \rho_f v^2 \left\{ \mathbf{J} + \frac{i\mu}{\omega} \mathbf{R} \right\} = \begin{bmatrix} M - \rho_f v^2 \left\{ J_{11} + \frac{i\mu}{\omega} R_{11} \right\} & 0 & 0 \\ 0 & -\rho_f v^2 \left\{ J_{22} + \frac{i\mu}{\omega} R_{22} \right\} & 0 \\ 0 & 0 & -\rho_f v^2 \left\{ J_{33} + \frac{i\mu}{\omega} R_{33} \right\} \end{bmatrix}. \quad (43)$$

Substitution of the four 3 by 3 matrices above into the 6 by 6 determinant (14) reveals that the result may be expressed as three 2 by 2 matrices for the three sets of components, $\{a_1, b_1\}$, $\{a_2, b_2\}$ and $\{a_3, b_3\}$:

$$\begin{bmatrix} Q_{11} - \rho v^2 & C_{11} - \rho_f v^2 \\ C_{11} - \rho_f v^2 & M - \rho_f v^2 \left\{ J_{11} + \frac{i\mu}{\omega} R_{11} \right\} \end{bmatrix} \begin{bmatrix} a_1 \\ b_1 \end{bmatrix} = 0, \\ \begin{bmatrix} Q_{22} - \rho v^2 & -\rho_f v^2 \\ -\rho_f v^2 & -\rho_f v^2 \left\{ J_{22} + \frac{i\mu}{\omega} R_{22} \right\} \end{bmatrix} \begin{bmatrix} a_2 \\ b_2 \end{bmatrix} = 0, \\ \begin{bmatrix} Q_{33} - \rho v^2 & -\rho_f v^2 \\ -\rho_f v^2 & -\rho_f v^2 \left\{ J_{33} + \frac{i\mu}{\omega} R_{33} \right\} \end{bmatrix} \begin{bmatrix} a_3 \\ b_3 \end{bmatrix} = 0. \quad (44)$$

Requiring that the determinants of these 2 by 2 matrices vanish yields four non-trivial solutions for the squared wave speed v^2 . The vanishing of the first of the determinants of these 2 by 2 matrices provides two roots of a quadratic equation that represent the fast and the slow squared longitudinal wave speeds. These speeds are given by

$$v^2 = \frac{\omega^2}{(k_1 + i\alpha_1)^2}, \quad (45)$$

where the specific formulas for calculating k_1 and α_1 require a hierarchy of substitutions specified by the following equations and the interposed text. k_1 and α_1 are given by

$$k_1 = \frac{1}{\sqrt{2}} \sqrt{\sqrt{k_0^2 + \alpha_0^2} + k_0}, \quad \alpha_1 = \frac{\text{sgn } \alpha_0}{\sqrt{2}} \sqrt{\sqrt{k_0^2 + \alpha_0^2} - k_0}, \quad (46)$$

where the two possible values of both k_0 and α_0 are given by

$$k_0 = \frac{2\rho\omega^2 \left[\left(J_{11} - \frac{\rho_f}{\rho} \right) \left(\frac{\rho}{\rho_f} M + J_{11} - 2C_{11} \pm k_{-1} \right) + \frac{\mu}{\omega} R_{11} \left(\frac{\mu}{\omega} R_{11} Q_{11} \pm \alpha_{-1} \right) \right]}{\left(\frac{\rho}{\rho_f} M + J_{11} - 2C_{11} \pm k_{-1} \right)^2 + \left(\frac{\mu}{\omega} R_{11} Q_{11} \pm \alpha_{-1} \right)^2}, \quad (47)$$

$$\alpha_0 = \frac{2\rho\omega^2 \left[\frac{\mu}{\omega} R_{11} \left(\frac{\rho}{\rho_f} M + J_{11} - 2C_{11} \pm k_{-1} \right) - \left(\frac{\mu}{\omega} R_{11} Q_{11} \pm \alpha_{-1} \right) \left(J_{11} - \frac{\rho_f}{\rho} \right) \right]}{\left(\frac{\rho}{\rho_f} M + J_{11} - 2C_{11} \pm k_{-1} \right)^2 + \left(\frac{\mu}{\omega} R_{11} Q_{11} \pm \alpha_{-1} \right)^2}, \quad (47)$$

where the two possible values are determined by selecting the + and – signs. The two roots correspond to the fast and the slow longitudinal waves. The k_{-1} and α_{-1} appearing in the formulas for k_0 and α_0 above are given by

$$k_{-1} = \frac{1}{\sqrt{2}} \sqrt{\sqrt{k_{-2}^2 + \alpha_{-2}^2} + k_{-2}}, \quad \alpha_{-1} = \frac{\text{sgn } \alpha_{-2}}{\sqrt{2}} \sqrt{\sqrt{k_{-2}^2 + \alpha_{-2}^2} + k_{-2}}, \quad (48)$$

where the k_{-2} and α_{-2} appearing in the equation above are given by

$$k_{-2} = \left(\frac{\rho}{\rho_f} M \right)^2 + 2C_{11}^2 \frac{\rho}{\rho_f} M + 2J_{11} \left(Q_{11} \left(\frac{\rho}{\rho_f} M - C_{11}^2 \right) + 2C_{11}^2 \frac{\rho}{\rho_f} \right) + (Q_{11})^2 \left\{ (J_{11})^2 - \left(\frac{\mu}{\omega} R_{11} \right)^2 \right\}, \quad (49)$$

$$\alpha_{-2} = 2 \frac{\mu}{\omega} R_{11} \left(Q_{11} \left(\frac{\rho}{\rho_f} M - C_{11}^2 \right) + J_{11} + 2C_{11}^2 \frac{\rho}{\rho_f} \right).$$

Fortunately the formulas for the shear waves are much simpler. The vanishing of the second and third of the determinants of the 2 by 2 matrices in (44) provide a zero root and a non-zero root from each determinant. The two non-zero roots are the squared shear wave speeds:

$$v^2 = \frac{Q_{22}}{\rho} \frac{J_{22} + \frac{i\mu}{\omega} R_{22}}{J_{22} - \frac{\rho_f}{\rho} + \frac{i\mu}{\omega} R_{22}} \quad \text{and} \quad v^2 = \frac{Q_{33}}{\rho} \frac{J_{33} + \frac{i\mu}{\omega} R_{33}}{J_{33} - \frac{\rho_f}{\rho} + \frac{i\mu}{\omega} R_{33}}. \quad (50)$$

When the first of these are recast in the form of (7), (45), k_2 and α_2 are given by

$$k_2 = \frac{\omega}{\sqrt{2} \frac{Q_{22}}{\rho}} \sqrt{\sqrt{\left\{ 1 - \frac{\frac{\rho_f}{\rho} J_{22}}{J_{22}^2 + \left(\frac{\mu}{\omega} R_{22} \right)^2} \right\}^2 + \frac{\left(\frac{\rho_f}{\rho} \frac{\mu}{\omega} R_{22} \right)^2}{\left(J_{22}^2 + \left(\frac{\mu}{\omega} R_{22} \right)^2 \right)^2}} + \left(1 - \frac{\frac{\rho_f}{\rho} J_{22}}{J_{22}^2 - \left(\frac{\mu}{\omega} R_{22} \right)^2} \right)}, \quad (51)$$

$$\alpha_2 = \frac{\omega}{\sqrt{2} \frac{Q_{22}}{\rho}} \sqrt{\sqrt{\left\{ 1 - \frac{\frac{\rho_f}{\rho} J_{22}}{J_{22}^2 + \left(\frac{\mu}{\omega} R_{22} \right)^2} \right\}^2 + \frac{\left(\frac{\rho_f}{\rho} \frac{\mu}{\omega} R_{22} \right)^2}{\left(J_{22}^2 + \left(\frac{\mu}{\omega} R_{22} \right)^2 \right)^2}} - \left(1 - \frac{\frac{\rho_f}{\rho} J_{22}}{J_{22}^2 + \left(\frac{\mu}{\omega} R_{22} \right)^2} \right)}$$

and similar formulas apply in the recasting of the second of (50); one need only replace the 2's by 3's in equation (51).

3.2. Wave polarization

The vectors \mathbf{a} and \mathbf{b} for the fast and slow waves are given by

$$\mathbf{a} = \{a_1, 0, 0\}, \quad \mathbf{b} = \{b_1, 0, 0\}, \quad (52)$$

where a_1 and b_1 are related by the following two equivalent expressions for the fast wave

$$a_1 = \frac{\rho_f(v_0^2 + c_0^2 - C_{11})}{\rho(v_0^2 + c_0^2) - \rho_f Q_{11}}, \quad (53)$$

$$b_1 = \frac{\left(J_{11} + \frac{i\mu}{\omega} R_{11}\right)(v_0^2 + c_0^2) - M}{v_0^2 + c_0^2 - C_{11}} b_1,$$

and the next two equivalent expressions for the slow wave,

$$a_1 = \frac{\rho_f(v_0^2 - c_0^2) - \rho_f C_{11}}{\rho(v_0^2 + c_0^2) - \rho_f Q_{11}}, \quad (54)$$

$$b_1 = \frac{\left(J_{11} + \frac{i\mu}{\omega} R_{11}\right)(c_0^2 - v_0^2) + M}{c_0^2 - v_0^2 + C_{11}} b_1,$$

and for the two shear waves by

$$\mathbf{a} = \{0, a_2, 0\}, \quad \mathbf{b} = \{0, b_2, 0\},$$

$$a_2 = -\left(J_{22} + \frac{i\mu}{\omega} R_{22}\right) b_2,$$

and

$$\mathbf{a} = \{0, 0, a_3\}, \quad \mathbf{b} = \{0, 0, b_3\},$$

$$a_3 = -\left(J_{33} + \frac{i\mu}{\omega} R_{33}\right) b_3,$$

respectively.

3.3. Numerical example applied to cancellous bone

The anisotropic poroelastic model of wave propagation is now applied to the case of cancellous bone, and these numerical results will be used to analyze fast and slow wave velocity measurements from bovine and human bone samples previously reported [12]. In order to apply the model to cancellous bone, values of the fluid and solid constituents of bone were obtained from the literature. Since the fluid saturating

the cancellous bone structure in our experiments is water, the fluid mass density $\rho^f = 1000 \text{ Kg/m}^3$, bulk modulus $K^f = 2.25 \text{ GPa}$ and viscosity $\mu = 1 \times 10^{-3} \text{ Pa-s}$. Furthermore, the mass density of the solid tissue in trabecular bone ρ^s has been reported to vary between 1800 and 2200 Kg/m^3 [27]–[29], depending on the tissue mineral density of the sample being measured. Likewise, the Young's elastic modulus of the mineralized matrix (E^s) has been determined using acoustic microscopy and nanoindentation [30]–[39], exhibiting values ranging from 11.4 to 22.7 GPa. Specifically, the E^s value measured in the circumferential direction varies between 13.5 and 16 GPa, and in the longitudinal direction the E^s value varies between 19 and 23 GPa. These values of E^s obtained at the subtrabecular scale are close to the classical values measured for cortical bone, which are 15 GPa in the circumferential direction and 20 GPa in the longitudinal direction. This large variability reported in the literature for E^s is certainly due to the intrinsic variability of the tissue mineralization and organic composition, but may also be a consequence of using estimation approaches based on different assumptions (boundary conditions, geometry, homogeneity), and experimental conditions (temperature, tissue dehydration, strain rate, size scale). The values for the material properties of the solid and fluid constituents of bone considered in our numerical results are summarized in the table.

Table. Bone tissue modulus, mass density and fluid viscosity of fluid in bone

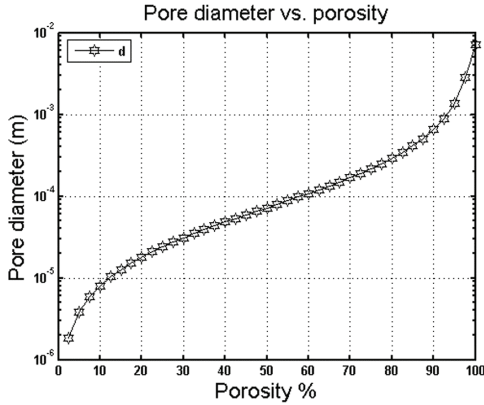
Parameter	Symbol	Value	Units
Young's elastic modulus of the solid	E^s	18	GPa
Mass density of the solid	ρ^s	2000	Kg/m^3
Mass density of the fluid	ρ^f	1000	Kg/m^3
Fluid bulk modulus	K^f	2.25	GPa
Fluid viscosity	μ	1×10^{-3}	Pa-s
Pore size–porosity proportionality constant	c	5×10^{-5}	m

In addition to the material properties of the solid and fluid constituents of bone, the model requires the value of the average, or effective, pore diameter d and the average intrinsic permeability κ_0 as a function of the porosity. Histomorphometrical studies on cancellous bone have reported pore sizes (trabecular spacing) ranging from 300 μm to 2200 μm for samples between 52 and 96% porosity [40]–[43]. Furthermore, the pore size in 5–10% porosity cortical bone tissue is considered to vary from around 20 to 60 μm , which corresponds to the pore size of the Haversian canals [44], [45]. Based on such bounds, the following em-

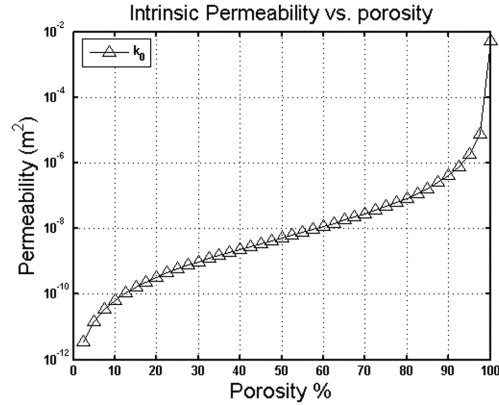
pirical relationship for the pore diameter d as a function of the porosity is proposed:

$$d(\phi) = c[\phi/(1-\phi)], \quad (56)$$

where c is a constant of proportionality, in this study chosen equal to 5×10^{-5} m, which leads to a variation of the pore diameter as a function of porosity (figure 1a)



a)



b)

Fig. 1. Pore diameter d as a function of porosity (a) and intrinsic permeability κ_0 as a function of porosity (b)

that corresponds to the bounds previously mentioned. It is important to notice that this is just an approximation to relate the variation of the average pore size with the porosity, but that such relationship may be different and much more complex. This aspect would be further explored in the near future by the authors.

Based on the pore size–porosity relationship (56), the dependence of the intrinsic permeability on the effective pore size $\kappa_0 = d^2$ [46] can be transformed to be dependent on the porosity as well $\kappa_0(\phi) = c^2[\phi/(1-\phi)]^2$. Predictions of the intrinsic permeability are shown in figure 1b, and exhibit a large variability that coincides with studies reporting experimental measurements of the permeability κ_0 (1×10^{-12} – 1×10^{-7} m²) on cancellous bone [47]–[54]. The variability of the intrinsic permeability in porous media is due to the dependence of the permeability on the porosity [48], [49] and the microstructure of the sample [49]–[52].

3.4. Phase velocity as a function of porosity

The phase velocities of the two longitudinal modes of wave propagation along the axes of symmetry of an isotropic bone specimen (figure 2a) and an orthotropic bone specimen (figure 2b) are shown as

functions of the porosity in figure 2. The fast wave velocity (squares) depicted in figure 2a linearly decreases as the porosity increases from zero to 80%; conversely, the slow wave velocity (diamonds) increases with the porosity within the same range of porosity. However, this *monotonic* behavior changes drastically for porosities higher than about 80%, and

the fast wave velocity becomes almost constant and independent of the porosity. At the same high porosity level, the slow wave velocity shows a clear inflexion, becoming inversely related to the porosity. It is important to notice that in addition to being independent of the porosity, the fast wave at high porosity exhibits velocity values equal to the wave propagation in the fluid saturating the pores, the velocity of sound in water ($v_{\text{fluid}} = 1480$ – 1500 m/s).

Figure 2b is presented to illustrate the much greater variability possible with an orthotropic material compared to the isotropic material illustrated in figure 2a. In figure 2b, the two longitudinal wave modes are shown propagating along all three axes of symmetry of an orthotropic bone sample. Anisotropy is characterized by three distinct principal values of fabric, F_1 , F_2 and F_3 , and their associated perpendicular directions. In figure 2b, note the variability of the fast wave for porosities lower than about 80% porosity for the three different directions, as well as in the variability of the slow wave at porosities higher than 80%, for the three directions. In contrast, the slow wave velocity below 80% porosity and fast wave velocity above 80% are practically insensitive to the anisotropy of the trabecular bone structure.

These theoretical results indicate that changes in both porosity and anisotropy are mainly shown in the fast wave velocity at low and mild porosities, while these changes are observed in the slow wave velocity

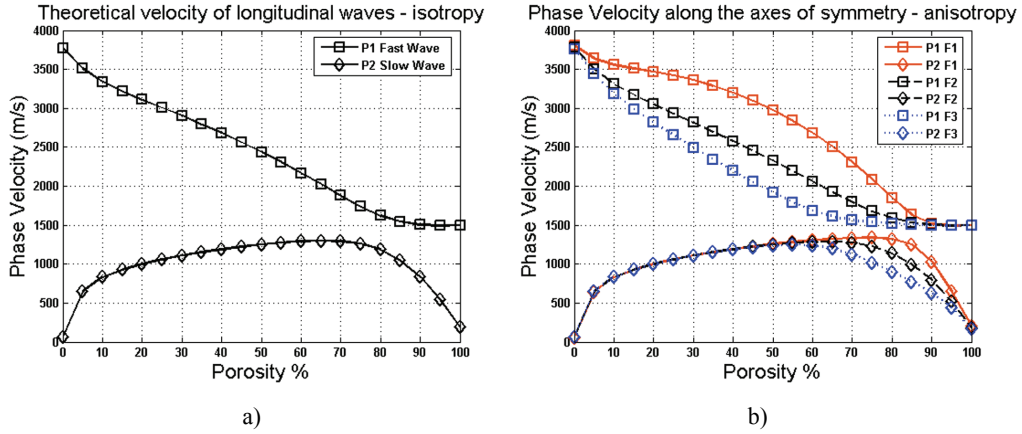


Fig. 2. Phase velocity as a function of porosity of the four wave modes in isotropic bone medium (a), and along the axes of symmetry in orthotropic bone sample (b)

mainly at high porosities. In contrast, the slow wave at low and mild porosities is slightly sensitive to changes in porosity and practically insensitive to bone anisotropy; and the fast wave at high porosities is independent of both porosity and anisotropy. Altogether, these findings indicate the existence of a *wave mode transition* between the longitudinal wave mode (fast or slow) that is most sensitive to changes in porosity and anisotropy.

Predictions of the fast and slow wave velocities made by this model will now be compared with experimental observations made previously by our group [12]. Briefly, fourteen bovine and sixty human trabecular bone samples were retrieved from bovine femoral heads, human femoral heads and femoral and tibial condyles. Ultrasound wave propagation measurements were obtained from the three orthogonal directions of these cubic shaped samples (A, B,

and C), thus taking into consideration the directional variability of the bone sample microarchitecture. Measurements were performed in immersion with distilled water at room temperature, using two broadband ultrasound transducers (Panametrics V323-SU) at a central frequency of 2.25 MHz (0.25 in diameter). The emitter was excited by a damped single pulse generated by an ultrasonic source (Panametrics 5052 UA) operated in a transmission mode. The signal was amplified in 40 dB and digitized by a 100 MHz Digital Oscilloscope (Tektronic model 2430) with a digitizing resolution of 10 bits and using a time window of 20.48 μ sec, and the post treatment data was performed in MATLAB.

Measurements of wave velocities obtained on three orthogonal directions on each sample were averaged and analyzed as a function of the porosity only (figure 3a). Figure 3b shows both the theoretical

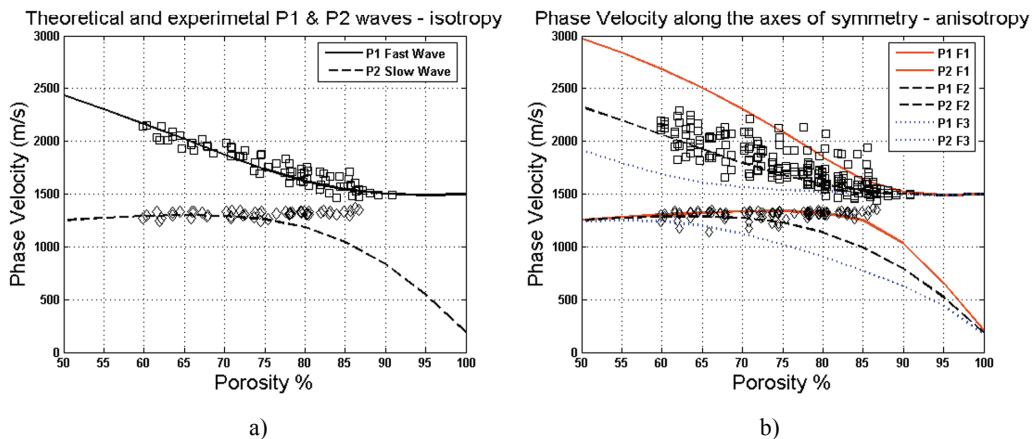


Fig. 3. Fast (squares) and slow (diamonds) wave velocities averaged over three orthogonal directions on each sample plotted as a function of bone porosity, compared to the theoretical fast (solid) and slow wave velocities (dashed) in isotropic medium (a); fast wave velocity (squares) and slow wave velocity data (diamonds) measured in three orthogonal directions on each sample plotted as a function of the measured bone porosity, and comparison with the theoretical fast (solid) and slow wave velocities (dashed) in anisotropic bone ($F_1 = 1.05$, $F_2 = 1.1$, $F_3 = 1.15$) (b)

predictions and experimental wave velocity measurements obtained on three orthogonal directions on each sample. The theoretical curves were computed for fabric anisotropy values F_1 , F_2 and F_3 equal to 1.05, 1.10 and 1.15, respectively. This choice of fabric anisotropy corresponds to the degree of anisotropy (5–17%) measured in the whole set of cancellous bone samples in our previous study [12]. Comparison of experimental data and theoretical results shows a *qualitative* agreement for both fast and slow wave measurements and these theoretical bounds. However, this last analysis is limited by the fact that the experimental data was obtained measuring the wave propagation in samples that were not cut aligned to their axes of symmetry. Therefore, the measured waves on those samples are

not pure wave modes, but quasi-waves. The development of the fabric-dependent anisotropic theory of propagation of quasi-waves in porous media will be presented in a separate study shortly, and a *quantitative* analysis of these experimental results would be performed.

Another important observation in our previous study of wave propagation in cancellous bone indicated that the fast wave is mostly related to the propagation in the solid structure and the slow wave is highly related to the fluid constituent [12]. Figure 4 shows a typical set of signals obtained in a single direction of a human sample: (i) a well-defined, single ultrasound wave excited the sample (figure 4a), (ii) the signal received after propagating through the

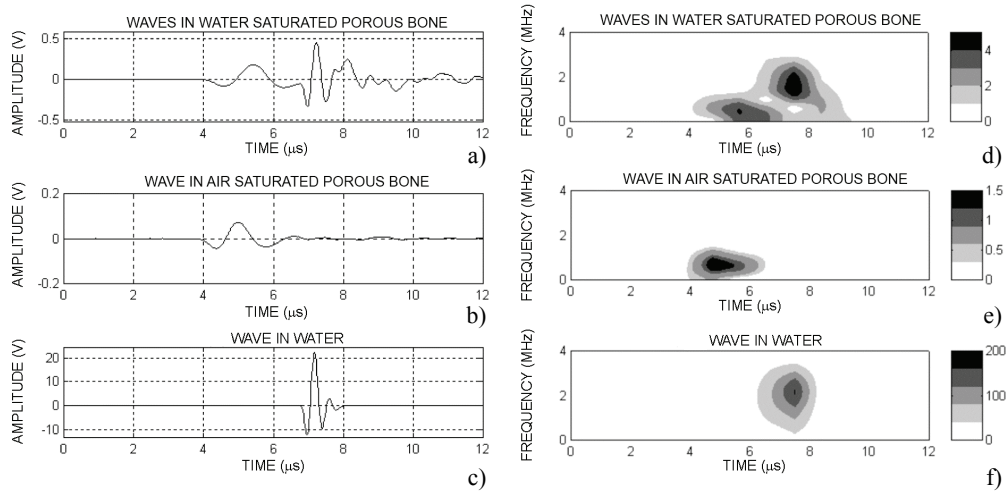


Fig. 4. Ultrasound wave after propagation through a fluid saturated human cancellous bone sample (a), signal propagation through the same human sample after the water was removed from the pores (b), detected pulse after propagating in water on a distance identical to the sample's size (c). Corresponding spectrograms of a human signal showing the two waves having different frequency compounds and time localization (d), when the fluid is removed from the pores (e) and when the porous sample is removed and the wave propagates in the fluid only (f). The color bar indicates the respective power spectra density value (V_{rms}^2)

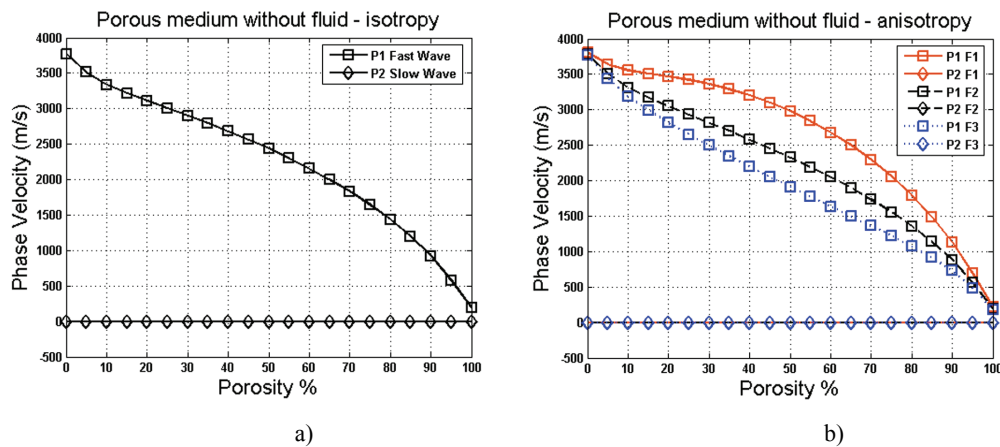


Fig. 5. Phase velocity as a function of porosity of the fast and slow wave modes in isotropic bone medium (a), and along the axes of symmetry in orthotropic bone sample (b) when the compressibility bulk modulus of the fluid is considered equal to zero. Under this condition the fluid does not contribute to the wave propagation

fluid-saturated cancellous bone sample (figure 4b), (iii) the signal received through the sample when the water medium was removed (figure 4c) and (iv) the signal received when the cancellous bone sample was removed, thus representing the propagation through the fluid alone (figure 4d). From these figures, it is clear that propagation through the cancellous bone structure dramatically alters the waveform, which after propagation is made of at least two distinguishable waves. When removing the water from the sample (figure 4c), only the very first part of the signal remains. On the contrary, when removing the sample while leaving the transducers in place, this first signal disappears and the remaining signal is very similar to the second part of the transmitted signal of figure 4b. From these results, one may conclude that the two waves observed with fluid saturated cancellous bone correspond in general to:

in the solid bony structure, while the slow wave is mostly related to the fluid saturating the pores, as illustrated in figures 2 and 3. The behavior of fast and slow waves above about 80% porosity follows the opposite trend, indicating that the fast wave is mostly related to the propagation in the fluid, and the slow wave is related to the solid bony structure. Both experimental measurements and theoretical predictions presented in this study indicate that the fast wave, when propagating in highly porous samples, is insensitive to the anisotropy of the cancellous bone structure and corresponds to the propagation in the fluid within the pores. **The clinical relevance of this finding is that the measurement of the fast wave, the wave measured by most clinical densitometers, lacks sensitivity to provide information on the bone structure when bone becomes osteoporotic.**

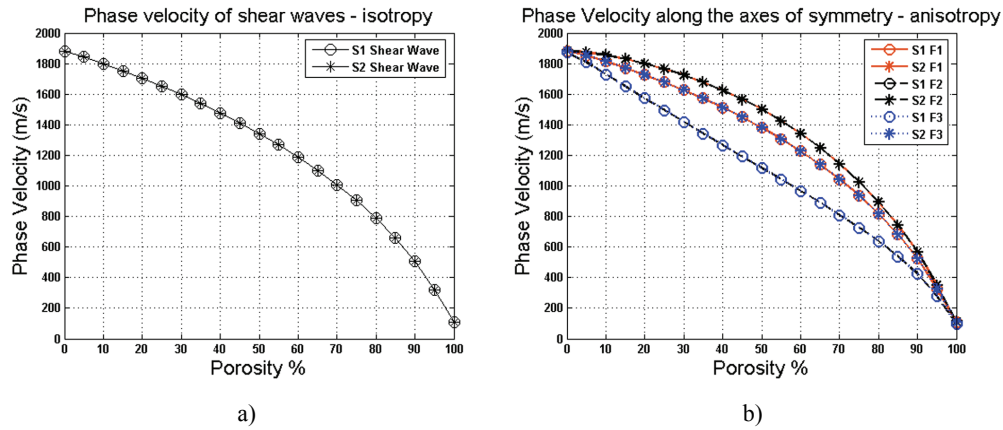


Fig. 6. Phase velocity as a function of porosity of the two shear wave modes in isotropic bone medium (a), and along the axes of symmetry in orthotropic bone samples (b)

(i) a first propagation mode related to the presence of a solid phase within the biphasic material and (ii) a second wave highly related to the effect of the fluid phase.

This observation is also verified by analyzing the wave propagation in the theoretical model when K_f tends to 0. Figure 5 shows the fast and slow wave velocities when the compressibility of the fluid tends to zero, for the isotropic (figure 5a) and the anisotropic cases (figure 5b). Here, the fluid does no longer contribute to the propagation of the waves, thus, the fast wave velocity is equivalent to the wave propagation velocity in the porous solid structure without fluid (as in figure 4c), and the slow wave does not propagate.

We return to the consideration of the wave mode transition that occurs for the fast wave at porosities below about 80% and it is related to the propagation

In addition to the longitudinal waves, the shear waves predicted by the theoretical model were analyzed. The two shear waves S1 (circles) and S2 (stars) have the exact same velocity in the isotropic case (figure 6a) and demonstrate a linear dependence on the medium's porosity. The two shear waves in the orthotropic medium exhibit a dependence on the bone's anisotropy, but smaller than the one observed in the fast or slow wave velocities (figure 6). However, the decrease in the S1 and S2 wave velocities as a function of porosity is monotonic within the whole range of porosity, and the bone structure anisotropy can be observed as shear wave velocity differences for the three analyzed directions (F_1 , F_2 and F_3). Since shear waves cannot propagate in the fluid, S1 and S2 velocities do not exhibit the change in behavior at about 80% porosity that is observed in the P1 and P2 longitudinal waves (figure 2).

3.5. Wave dispersion as a function of frequency

Figure 7 shows both the fast and slow wave velocities as a function of frequency for different values of porosity (figures 7a, c, e) and fabric (figures 7b, d, f). In figure 7a, the acoustic dispersion of all four wave-modes is depicted for a 50% porosity isotropic bone sample. A strong positive dispersion (velocity increasing with frequency) behavior is observed below the critical frequency in the slow wave. The dispersion of the fast wave is practically negligible at this porosity level, and the velocity of both fast and slow waves is constant at frequencies higher than the critical frequency. Figure 7c depicts the wave dispersion

in an isotropic bone sample with 70% porosity. This figure shows tendencies that are similar to the ones shown in figure 7a, but differs in that the velocities of the fast and shear waves are smaller than the wave velocities in the 50% porosity medium. Also, a slight dispersion in the fast wave velocity can be observed around the critical frequency value, and the slow wave transition from zero to a constant velocity value occurs around the same frequency. Figure 7e, for a 90% porosity isotropic medium, demonstrates that in a highly porous medium, both slow and fast waves are strongly dispersive. Even more interesting, there also exists a *wave mode transition* between the slow and the fast wave occurring around the critical frequency. The slow wave has a zero velocity at low frequencies (does not propagate) and above zero it starts propa-

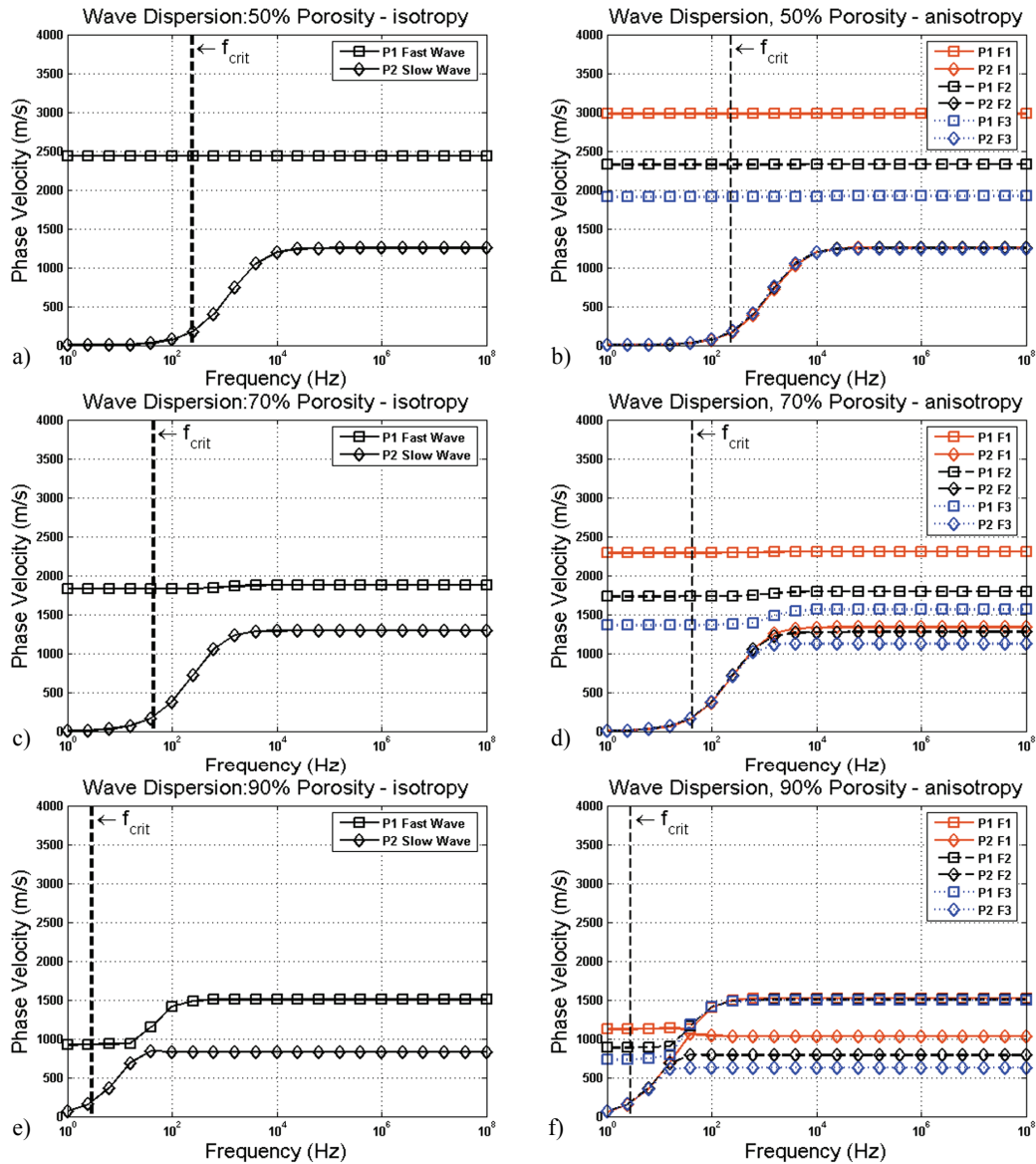


Fig. 7. Wave dispersion of fast and slow longitudinal modes in an isotropic porous media with 50% (a), 70% (c) and 90% porosity (e); as well as in an anisotropic media at 50% (b), 70% (d) and 90% porosity (f)

gating with a low speed that increases with the frequency. However, this dispersive behavior of the slow wave changes drastically and its velocity becomes constant for higher frequencies (the curve with diamonds). The fast wave, in turn, has the opposite behavior. It has a constant velocity at low frequencies and a sharp change in dispersion occurs at exactly the same frequency the slow wave dispersion changes. Moreover, it must be noted that, in all cases, the slow wave velocity tends to zero as the frequency of the wave approaches zero. At frequencies much higher than the critical frequency, the fast wave has a constant velocity, which is in fact equal to the velocity in the fluid phase of the porous medium, in this case 1480–1500 m/s.

The observations characterized by diamonds in figures 7a, 7c and 7e are also distinguished in figures 7b, 7d and 7f, with the difference that these last include the role of anisotropy. For each wave mode a set of three curves is produced; the three curves represent the wave propagation along the dynamic axes of symmetry in an orthotropic bone sample (F_1 , F_2 and F_3). In figure 7b, one can distinguish that the fast and shear waves exhibit changes in their respective velocities as a consequence of the anisotropy. Anisotropy has a mild effect on the slow wave velocity when the porosity is 50%. The effect of the anisotropy on the fast and shear waves is smaller when the porosity increases (figure 7e), and a little more pronounced in the slow wave than before. Figure 7f, which corresponds to a 90% porosity of anisotropic medium, shows again a wave mode transition between the fast and slow waves. The fast wave is non-dispersive and sensitive to the anisotropy at low frequencies, while the slow wave becomes the non-dispersive wave mode and sensitive to anisotropy at high frequencies. After the critical frequency, the fast wave becomes dispersive until it reaches the velocity of propagation of sound in the fluid. In contrast to longitudinal waves, the shear waves are non-dispersive but sensitive to the medium's anisotropy.

The critical frequency f_{crit} changes with both the porosity and the fabric anisotropy. This result demonstrates that the transition in the wave mode from non-dispersive to dispersive is an indicator of the porosity in the medium. The critical frequency, and thus the dispersive/non-dispersive behavior of longitudinal waves, also changes for the three analyzed directions in the anisotropic cancellous bone. In theory, above the critical frequency $f_{\text{crit}} = \mu / \pi \rho^f d^2$, both fast and slow waves may be expected to propagate.

Overall, this analysis demonstrates that the acoustic dispersion and the transition between the fast and

slow wave modes depend on both the porosity and the fabric anisotropy. These structural parameters and the viscosity of the fluid determine the magnitude of the viscous friction between the solid and the fluid constituents, and thus the frequency in which the transition between the low and high frequency domains of Biot's theory occurs.

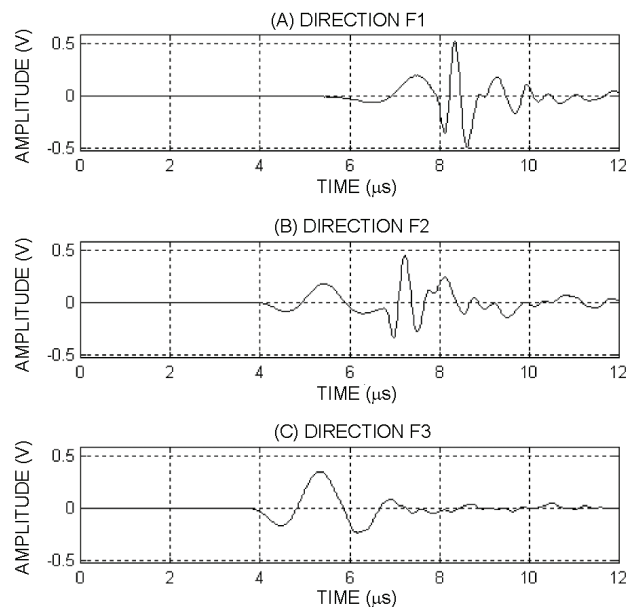


Fig. 8. Ultrasound waves propagated in three orthogonal directions of the same specimen. Only one wave was observed in the third direction. This observation is related to a high attenuation of the slow wave in this direction

The theoretical results shown in figures 2, 3 and 7 could explain our experimental observations that the slow wave may not be observed at the three orthogonal directions (A, B and C) of the same specimen. We have hypothesized [12] that two reasons could explain this observation: (i) the two waves superimpose in the time domain or (ii) the amplitudes of the fast and slow waves are very different and settings of the electronics did not allow observing both of them simultaneously. Superimposition of the fast and slow waves was clearly observed in some of the samples, as shown in figure 8: in the B direction both waves were observed and could be easily distinguished, while in the A direction, the two waves were found closer to each other and pulses difficult to isolate. This behavior of wave superposition was also observed in HOSOKAWA's work [10] when changing the ultrasonic propagation direction within the sample. The anisotropic theoretical model predicts specific conditions of porosity and fabric for which the velocities of the fast and slow wave modes are almost identical, thus supporting the first interpretation.

3.6. Wave attenuation as a function of porosity or frequency

The ultrasonic attenuation coefficient α represents the amount of energy lost by the ultrasonic beam

The attenuation of longitudinal waves as a function of porosity is shown in figure 9a for isotropic, and in 9c for an anisotropic bone sample of 1-cm size ($x_2 - x_1 = 1$ cm) calculated at 1 MHz. Attenuation of the fast wave (squares) is smaller than the attenuation of the slow wave at porosities below

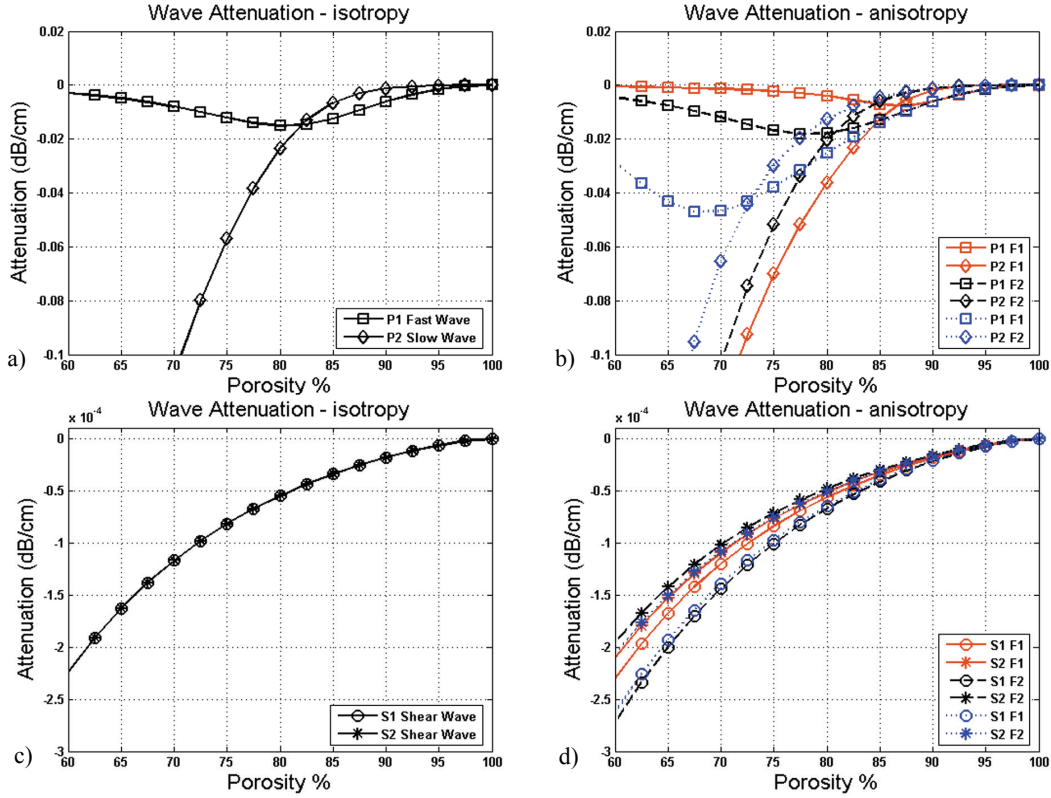


Fig. 9. Attenuation of longitudinal (a and c) and shear waves (b and d) as a function of porosity in isotropic bone media (a and b), and along the axes of symmetry (F_1 , F_2 and F_3) in orthotropic bone sample (c and d)

during its propagation through the medium due to absorption. In porous media, the solution of the poroelastic Christoffel equation gives complex roots since absorption is considered in the model. The complex wave number defines the attenuation coefficient α for the corresponding wave mode

$$K_{\text{Re}} + i\alpha_{\text{Im}} = \frac{\omega}{v_{\text{Re}} + iv_{\text{Im}}} = \frac{\omega v_{\text{Re}}}{(v_{\text{Re}})^2 + (v_{\text{Im}})^2} - i \frac{\omega v_{\text{Im}}}{(v_{\text{Re}})^2 + (v_{\text{Im}})^2}, \quad (57)$$

$$\alpha_{\text{Im}} = - \frac{\omega v_{\text{Im}}}{(v_{\text{Re}})^2 + (v_{\text{Im}})^2} \quad (58)$$

and

$$Att_{dB}(\omega) = -20 \log(e)(x_2 - x_1)\alpha_{\text{Im}}. \quad (59)$$

about 80%. However, the attenuation of both waves changes in behavior above about 80%, and the slow wave becomes slightly less attenuated than the fast wave (figure 9a). The porosity at which this transition between fast and slow wave occurs is however affected by the fabric anisotropy, as shown in figure 9b. This observation indicates that there exist a range of porosity and anisotropy where the absorption-related attenuation for both waves is of the same order of magnitude. Therefore, whether both waves may have similar amplitude and might be observed simultaneously depends on both the porosity and anisotropy of the sample.

In addition to the role of the porosity and fabric anisotropy, the dependence of attenuation on frequency was analyzed. The attenuation of longitudinal waves versus frequency is shown in figure 10a for isotropic, and in 10b for an anisotropic bone sample

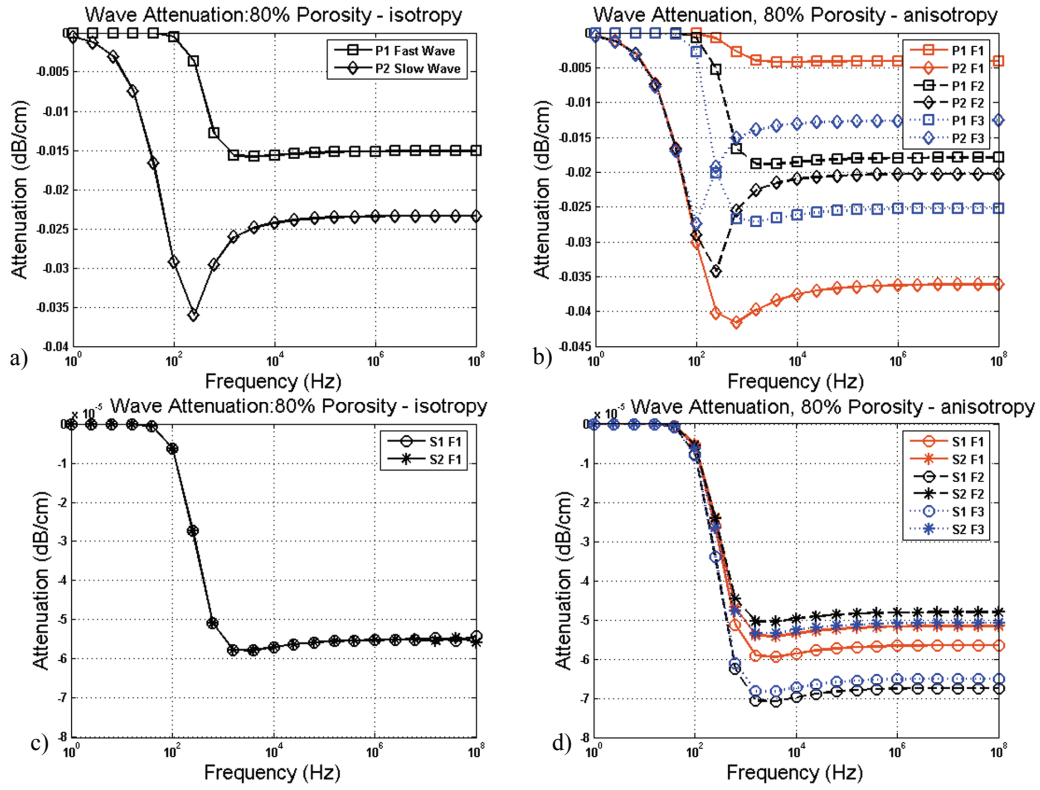


Fig. 10. Wave attenuation as a function of frequency of the fast and slow wave modes in isotropic bone medium (a), along the axes of symmetry (F_1 , F_2 and F_3) in orthotropic bone sample (c), Shear wave modes in isotropic bone medium (b), and shear waves along the axes of symmetry (F_1 , F_2 and F_3) in orthotropic bone sample (d)

of 1-cm size and 80% porosity. Attenuation of the fast wave (squares) is smaller than the attenuation of the slow wave at low frequencies. However, the attenuation of both waves changes in behavior, and the slow wave becomes slightly less attenuated than the fast wave at high frequencies (figure 10a). The frequency at which this transition between fast and slow wave occurs is determined by the pore diameter, fluid density and viscosity. Figure 10b shows that the transition in attenuation between the fast and slow wave also depends on the fabric. The transition in attenuation between the fast and slow waves only occurs at direction F_1 , but not in F_2 and F_3 , for which the slow wave remains the most attenuated for all frequencies.

The implication of these results is that both the porosity and the fabric play a critical role in the absorption-dependent attenuation of longitudinal waves. This theoretical result is also a plausible explanation for the observation of two waves with a high difference in their respective amplitude. Figure 11 provides a signal obtained with a highly porous sample where the fast wave is almost undetectable. This fast wave still existed, as demonstrated in figure 11b where the signal was magnified, and its amplitude was about 30 times lower than that of the slow wave.

The theoretical results shown in figure 9 indicate that the fast wave can be more attenuated than the slow wave at certain conditions of porosity and fabric, and could explain our experimental observations that one of the two waves may be overlooked and remain unmeasured. In figure 11, the undetected wave is the fast mode, and in figure 8c is the slow wave. Superimposition of the fast and slow waves was thus clearly predicted by the anisotropic poroelastic model.

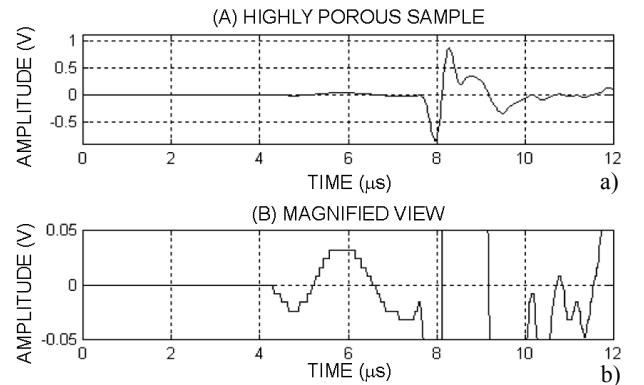


Fig. 11. Case of signals detected in a very porous sample where (a) the fast wave was almost imperceptible, (b) a higher magnification showing the existence of the fast wave

4. Discussion

Anisotropic poroelastic wave propagation theory was extended in this study by introducing the dependence of the wave motion equations upon fabric, a tensorial descriptor of the porous microarchitecture. Solution of the constitutive equations for harmonic displacements of the solid and fluid constituents leads to a modified Christoffel equation for anisotropic porous media that includes the acoustic tensor \mathbf{Q} , the solid–fluid interaction tensor \mathbf{C} , and the permeability tensor $\mathbf{K}(\omega)$. These tensors describe the elastic and viscous effects in the wave equation, and they all depend on the measurable fabric tensor, \mathbf{F} . The modified Christoffel equation represents an eigenvalue problem with the sixth order characteristic equation and four non-zero roots. This system reduces to the isotropic formulation developed by Biot when the fabric tensor is isotropic. Two eigenvalues represent the longitudinal wave modes P1 and P2 and the other two correspond to the shear wave modes S1 and S2. Such eigenvalues are complex valued, and describe the phase velocity and attenuation due to absorption of the four wave modes.

Propagation of plane waves in both isotropic and anisotropic saturated porous media was analyzed as a function of the porosity and fabric. Elastic constant and density values for the mineralized bone tissue and water were used in the poroelastic model to study the wave propagation in cancellous bone. Two constants are used to describe the solid phase (E^s and ρ^s), three for the fluid phase (ρ^f , K^f and μ) and one constant to relate the porosity to the pore diameter. Two independent variables (ϕ and \mathbf{F}), one scalar and the other tensorial, respectively, were integrated in the model to study the influence of material properties on both global and directional changes in the velocity and attenuation of the four wave modes generated in porous media.

The theoretical model predicted that in isotropic media with porosity below 80%, the fast wave decreases with the porosity. At porosities higher than 80%, the fast wave exhibits a constant velocity, and the slow wave is the wave mode that is sensitive to changes in porosity. This result demonstrated that one of the two wave modes is more sensitive than the other to changes in porosity; however, there exists a transition in sensitivity between the two longitudinal wave modes at approximately 80% porosity. The fast wave is sensitive to the porosity when the apparent modulus to density ratio of the solid phase ($(1 - \phi)K^s/\rho^s$) is higher than that of the fluid phase

($\phi K^f/\rho^f$); while the slow wave is sensitive to porosity when the apparent modulus to density ratio of the solid phase is smaller than that of the fluid phase. Therefore, the porosity level at which this transition between the fast and the slow wave modes occurs is a consequence of the intrinsic properties of the solid (E^s and ρ^s) and fluid (ρ^f , K^f and μ) constituents. For instance, if the properties for the fluid phase are changed to those of glycerol ($\rho^f = 1261 \text{ Kg/m}^3$, $K^s = 4.35 \text{ GPa}$, and $\mu = 1.5 \text{ Pa-s}$), the transition between the wave modes happens at 65% and with ethanol at 20 °C ($\rho^f = 789 \text{ Kg/m}^3$, $K^f = 0.902 \text{ GPa}$, and $\mu = 1.2 \times 10^{-3} \text{ Pa-s}$), the transition between the wave modes happens at 90% (figure not shown). The shear wave modes, in contrast, are not affected by the presence of the fluid and do not exhibit a change in behavior as shown in the longitudinal waves. Shear waves are, however, sensitive to both porosity and anisotropy.

It is important to note that the porosity at which the fast wave–slow wave mode transition occurs in longitudinal waves depends on the fabric anisotropy. The theoretical model predicted that mild changes in anisotropy would produce this transition to occur in the porosity range between 70% and 90%. In an orthotropic bone sample, the direction with lower modulus will exhibit a transition at a lower porosity than the direction with intermediate and high modulus. Consequently, this theoretical model indicates that an anisotropic bone sample with approximately 80% porosity may exhibit either a fast or slow wave that is sensitive or insensitive to the anisotropy of the medium, depending on the direction being analyzed.

The wave mode transition observed in the analysis of velocity as a function of porosity and fabric anisotropy is also observed when the wave velocity is analyzed as a function of the frequency. The wave mode transition occurs around the critical frequency in samples with high porosity (>80%). The fast and slow wave dispersion changes drastically in behavior at the frequency where the velocity (and the wave length) of both wave modes becomes very similar. However, the frequency at which this transition occurs is also affected by the fabric anisotropy. Therefore, the transition frequency from being non-dispersive to dispersive and vice versa is a consequence of the intrinsic and extrinsic properties of the medium (material constituents, porosity and fabric anisotropy). The transition between the low and high frequency regimes defined by Biot (critical frequency) at which the slow wave becomes a propagative wave mode occurs at frequencies much lower than the ones usually employed for ultrasound characterization of bone. In fact,

the model predicted very low acoustic dispersion into the range of porosity, fabric and frequencies generally used in clinical applications. It is important to notice that the wave dispersion predicted by the model is a consequence of the absorption in either isotropic media or in anisotropic media along the dynamic axes of the sample. However, dispersion processes may be more complex when the wave propagation is analyzed in directions that are not normal to planes of material symmetry.

The theoretical model also predicted the high variability of fast and slow wave velocities observed in bovine and human bones in our experimental study. Comparison of experimental data and theoretical results shows a qualitative agreement for both fast and slow wave velocities. Directional variability within a sample was effectively explained by the theoretical model after inclusion of the fabric; this directional variability could not be explained by the porosity only. The agreement between experimental and theoretical values in this study indicates that despite the complexity added to the poroelastic theory, a tensorial variable describing the bone microstructure is required to explain the directional variability of the wave propagation with bone architecture. Nonetheless, the comparison between experiments and theoretical predictions in this study is limited by the fact that the experimental data was obtained measuring the wave propagation in samples that were not cut aligned to their axes of symmetry. Therefore, the measured waves on those samples are not pure wave modes, but quasi-waves. The development of the fabric-dependent anisotropic theory of propagation of quasi-waves in porous media will be presented in a separate study, and a *quantitative* analysis of these experimental results will be performed. Moreover, solid and fluid interaction phenomena should be thoroughly investigated. For this reason, studies of ultrasonic wave propagation properties using various solid porous materials mimicking cancellous bone structure as well as various saturating fluids exhibiting different physical properties (elasticity, density, viscosity) are needed.

The analysis of the wave attenuation as a function of the porosity, fabric and frequency demonstrated that there exists a range of porosity and anisotropy – at a given fixed frequency – in which the attenuation due to absorption is of the same order of magnitude for both fast and slow wave modes. Similarly to the longitudinal wave velocities, a transition in the attenuation of the two wave modes occurs around 80% in an isotropic medium and within the 70% to 90% range when anisotropy is considered. The important implication of this theoretical result is that, depending on

the porosity and the fabric anisotropy of the sample, one wave mode – either the fast or the slow – may be highly attenuated with respect to the other and remain practically undetected as shown in our experimental study. Notice that the fast to slow wave attenuation ratio depends on the porosity and fabric anisotropy. In other words, the direction in which the sample is interrogated may not allow a clear observation of both waves simultaneously if they superimpose due to having similar velocities or having very different attenuations. This may explain why the clinical densitometer systems measuring the wave propagation in the medial-lateral direction at the calcaneum might not be able to distinguish, thus far, both waves in vivo. Usually, velocity and attenuation measurement methods (in clinical densitometers) presuppose that only one wave propagates in cancellous bone. However, if only one wave is observable/measurable at a given direction, then it is even more important to distinguish whether that wave is the fast or the slow wave mode, and whether that wave mode is sensitive or not to the anisotropy of the cancellous porous structure.

Overall, the results from the present study demonstrate the ability of the proposed model to describe the acoustic behavior of the fast and slow wave velocities in cancellous bone. Both phase velocity and attenuation are dependent on the architecture (porosity and fabric) and the composition of the medium (solid and fluid mass density, solid elastic modulus, fluid bulk modulus and fluid viscosity). For given frequency and material parameter values, the behaviors of the fast and slow waves are governed by the extrinsic properties of the media: the porosity and fabric anisotropy. These theoretical predictions also corroborate our experimental observations which indicate that at high porosities the fast wave is mostly related to the propagation in the fluid constituent and the slow wave is highly related to the solid structure. ***Therefore, the theoretical predictions confirm our observations that the measurement of the fast wave lacks sensitivity to provide information on the bone structure when bone becomes osteoporotic.*** In contrast to empirical relationships used by ultrasound densitometers, the fabric-dependent anisotropic poroelastic model proposed in this study provides a theoretical framework to predict, analyze and interpret changes in elastic constants of the trabecular bone structure. Since the velocity and attenuation predictions provided by this novel approach depend on the tissue composition, porosity and architecture of the cancellous bone sample, it has the potential to characterize bone quality beyond BMD.

Acknowledgements

This work was supported by the National Institutes of Health (AG34198 & HL069537-07 R25 Grant for Minority BME Education), the National Science Foundation (NSF 0723027, PHY-0848491), and the PSC-CUNY Research Award Program of the City University of New York.

References

- [1] COWIN S.C., CARDOSO L., *Fabric dependence of poroelastic wave propagation*, Biomechan. Model Mechanobiol., 2010, in press, Online First, Open Access.
- [2] SIFFERT R., KAUFMAN J., *Ultrasonic bone assessment: "The time has come"*, Bone, 2006, Vol. 40, Issue 1, Page 5.
- [3] HANS D., FUERST T., UFFMANN M., *Bone density and quality measurement using ultrasound*, Curr. Opin. Rheumatol., 1996, 8, 370–375.
- [4] GRIMM M.J., WILLIAMS J.L., *Assessment of bone quantity and 'quality' by ultrasound attenuation and velocity in the heel*, Clin. Biomech. (Bristol, Avon), 1997a, 12, 281–285.
- [5] GRIGORIAN M., SHEPHERD J.A., CHENG X.G., NJEH C.F., TOSCHKE J.O., GENANT H.K., *Does osteoporosis classification using heel BMD agree across manufacturers?* Osteoporos Int., 2002, 13, 613–617.
- [6] NJEH C.F., FUERST T., DIESSEL E., GENANT H.K., *Is quantitative ultrasound dependent on bone structure? A reflection*, Osteoporos. Int., 2001, 12, 1–15.
- [7] NICHOLSON P.H.F., MÜLLER R., LOWET G., CHENG X.G., HILDEBRAND T., RÜEGSEGGER P., VAN DER PERRE G., DEQUEKER J., BOONEN S., *Do quantitative ultrasound measurements reflect structure independently of density in human vertebral cancellous bone?* Bone, 1998, 23, 425–431.
- [8] SAKATA S., BARKMANN R., LOCHMULLER E.M., HELLER M., GLUER C.C., *Assessing bone status beyond BMD: evaluation of bone geometry and porosity by quantitative ultrasound of human finger phalanges*, J. Bone Miner. Res., 2004, 19, 924–930.
- [9] HOSOKAWA A., OTANI T., *Ultrasonic wave propagation in bovine cancellous bone*, J. Acoust. Soc. Am., 1997, 101, 558–562.
- [10] HOSOKAWA A., OTANI T., *Acoustic anisotropy in bovine cancellous bone*, J. Acoust. Soc. Am., 1998, 103, 2718–2722.
- [11] CARDOSO L., TEBOUL F., MEUNIER A., ODDOU C., *Ultrasound Characterization of Cancellous Bone: Theoretical and Experimental Analysis*, Transactions of the ultrasonics symposium, IEEE, 2001, Vol. 2, 1213–1216.
- [12] CARDOSO L., TEBOUL F., SEDEL L., MEUNIER A., ODDOU C., *In vitro acoustic waves propagation in human and bovine cancellous bone*, Journal of Bone and Mineral Research, 2003, 18 (10), 1803–1812.
- [13] BIOT M.A., *General theory of three-dimensional consolidation*, J. Appl. Phys., 1941, 12, 155–164.
- [14] BIOT M.A., *Theory of elasticity and consolidation for a porous anisotropic solid*, J. Appl. Phys., 1955, 26, 182–182.
- [15] BIOT M.A., *Theory of propagation of elastic waves in a fluid saturated porous solid I low frequency range*, J. Acoust. Soc. Am., 1956a, 28, 168–178.
- [16] BIOT M.A., *Theory of propagation of elastic waves in a fluid saturated porous solid II higher frequency range*, J. Acoust. Soc. Am., 1956b, 28, 179–191.
- [17] BIOT M.A., *Mechanics of deformation and acoustic propagation in porous media*, J. Appl. Phys., 1962a, 33, 1482–1498.
- [18] BIOT M.A., *Generalized theory of acoustic propagation in porous dissipative media*, J. Acoust. Soc. Am., 1962b, 28, 1254–1264.
- [19] COWIN S.C., *The relationship between the elasticity tensor and the fabric tensor*, Mech. Mater., 1985, 4, 137–147.
- [20] PLONA T.J., JOHNSON D.L., *Acoustic properties of porous systems: I. phenomenological description*, [in:] *Physics and Chemistry of porous media*, AIP Conference Proceedings, 1983, No. 107 (Johnson D.L. and Sen P.N. eds.), 89–104.
- [21] WILLIAMS J.L., *Ultrasonic wave propagation in cancellous and cortical bone: Prediction of some experimental results by Biot's theory*, J. Acoust. Soc. Am., 1992, 91, 1106–1112.
- [22] CARDOSO L., MEUNIER A., ODDOU C., *In vitro acoustic wave propagation in human and bovine cancellous bone as predicted by the Biot's theory*, Journal of Mechanics in Medicine and Biology, 2008, Vol. 8, No. 2, 1–19.
- [23] MASON W.P., *Physical acoustics and the properties of solids*, Van Nostrand Reinhold, Princeton, 1958.
- [24] AULD B., *Acoustic Fields and Waves in Solids*. Vol. 1, John Wiley and Sons, New York, London, Sidney, Toronto, 1973.
- [25] JOHNSON D.L., PLONA T.J., *Acoustic slow waves and the consolidation transition*, J. Acoust. Soc. Am., 1982, 72, 556–565.
- [26] PERROT C., CHEVILLOTTE F., PANNETON R., ALLARD J.-F., LAFARGE D., *On the dynamic viscous permeability tensor symmetry*, J. Acoust. Soc. Am. Express Letters, 2008, 124, EL210–217.
- [27] ASHMAN R.B., RHO J.Y., *Elastic modulus of trabecular bone material*, J. Biomech., 1988, 21, 77–181.
- [28] NICHOLSON P.H., CHENG X.G., LOWET G., BOONEN S., DAVIE M.W., DEQUEKER J., VAN DER PERRE G., *Structural and material mechanical properties of human vertebral cancellous bone*, Med. Eng. Phys., 1997, 19, 729–737.
- [29] MORGAN E.F., BAYRAKTAR H.H., KEAVENY T.M., *Trabecular bone modulus–density relationships depend on anatomic site*, J. Biomech., 2003, 36, 897–904.
- [30] TURNER C.H., RHO J., TAKANO Y., TSUI T.Y., PHARR G.M., *The elastic properties of trabecular and cortical bone tissues are similar: results from two microscopic measurement techniques*, J. Biomech., 1999, 32, 437–441.
- [31] JORGENSEN C.S., KUNDU T., *Measurement of material elastic constants of trabecular bone: a micromechanical analytic study using a 1 GHz acoustic microscope*, J. Orthop. Res., 2002, 20, 151–158.
- [32] RHO J.Y., TSUI T.Y., PHARR G.M., *Elastic properties of human cortical and trabecular lamellar bone measured by nanoindentation*, Biomaterials, 1997, 18, 1325–1330.
- [33] RHO J.Y., ROY M.E. 2ND, TSUI T.Y., PHARR G.M., *Elastic properties of microstructural components of human bone tissue as measured by nanoindentation*, J. Biomed. Mater. Res., 1999, 45, 48–54.
- [34] ROY M.E., RHO J.Y., TSUI T.Y., EVANS N.D., PHARR G.M., *Mechanical and morphological variation of the human lumbar vertebral cortical and trabecular bone*, J. Biomed. Mater. Res., 1999, 44, 191–197.
- [35] ZYSSET P.K., GUO X.E., HOFFLER C.E., MOORE K.E., GOLDSTEIN S.A., *Elastic modulus and hardness of cortical and trabecular bone lamellae measured by nanoindentation in the human femur*, J. Biomech., 1999, 32, 1005–1012.

- [36] HOFFLER C.E., MOORE K.E., KOZLOFF K., ZYSSET P.K., GOLDSTEIN S.A., *Age, gender, and bone lamellae elastic moduli*, J. Orthop. Res., 2000a, 18, 432–437.
- [37] HOFFLER C.E., MOORE K.E., KOZLOFF K., ZYSSET P.K., BROWN M.B., GOLDSTEIN S.A., *Heterogeneity of bone lamellar-level elastic moduli*, Bone, 2000b, 26, 603–609.
- [38] HENGESBERGER S., KULIK A., ZYSSET P., *A combined atomic force microscopy and nanoindentation technique to investigate the elastic properties of bone structural units*, Eur. Cell. Mater., 2001, 1, 12–17.
- [39] HENGESBERGER S., KULIK A., ZYSSET P., *Nanoindentation discriminates the elastic properties of individual human bone lamellae under dry and physiological conditions*, Bone, 2002, 30, 178–184.
- [40] PARFITT A.M., MATHEWS C.H., VILLANUEVA A.R., KLEERKOPER M., FRAME B., RAO D.S., *Relationships between surface, volume, and thickness of iliac trabecular bone in aging and in osteoporosis. Implications for the micro-anatomic and cellular mechanisms of bone loss*, J. Clin. Invest., 1983, 72(4), 1396–1409.
- [41] REHMAN M.T., HOYLAND J.A., DENTON J., FREEMONT A.J., *Age related histomorphometric changes in bone in normal British men and women*, J. Clin. Pathol., June, 1994, 47(6), 529–534.
- [42] HILDEBRAND T., LAIB A., MÜLLER R., DEQUEKER J., RÜEGSEGGER P., *Direct three-dimensional morphometric analysis of human cancellous bone: microstructural data from spine, femur, iliac crest, and calcaneus*, Journal of Bone and Mineral Research, 1999, 14, 1167–1174.
- [43] GLORIEUX F.H., TRAVERS R., TAYLOR A., BOWEN J.R., RAUCH F., NORMAN M., PARFITT A.M., *Normative data for iliac bone histomorphometry in growing children*, Bone, 2000, 26(2), 103–109.
- [44] JONES A.C., SHEPPARD A.P., SOK R.M., ARNS C.H., LIMAYE A., AVERDUNK H., BRANDWOOD A., SAKELLARIOU A., SENDEN T.J., MILTHORPE B.K., KNACKSTEDT M.A., *Three-dimensional analysis of cortical bone structure using X-ray micro-computed tomography*, Physica A: Statistical Mechanics and its Applications. 2004, Vol. 339, Issues 1–2, 125–130. Proceedings of the International Conference New Materials and Complexity.
- [45] BASILLAIS A., BENSAMOUN S., CHAPPARD CH., BRUNET-IMBAULT B., LEMINEUR G., ILHARREBORDE B., HO BA THO M.C., BENHAMOU C.L., *Three-dimensional characterization of cortical bone microstructure by microcomputed tomography: validation with ultrasonic and microscopic measurements*, Journal of Orthopaedic Science, 2007, 12, No. 2.
- [46] BEAR J., *Dynamics of Fluids in Porous Media*, Dover, 1988, p. 134.
- [47] LIM T.H., HONG J.H., *Poroelastic properties of bovine vertebral trabecular bone*, J. Orthop. Res., 2000, 18, 671–677.
- [48] GRIMM M.J., WILLIAMS J.L., *Measurements of permeability in human calcaneal trabecular bone*, J. Biomech., 1997b, 30, 743–745.
- [49] NAUMAN E.A., FONG K.E., KEAVENY T.M., *Dependence of intertrabecular permeability on flow direction and anatomic site*, Ann. Biomed. Eng., 1999, 27, 517–524.
- [50] KOHLES S.S., ROBERTS J.B., UPTON M.L., WILSON C.G., BONASSAR L.J., SCHLICHTING A.L., *Direct perfusion measurements of cancellous bone anisotropic permeability*, J. Biomech., 2001, 34, 1197–1202.
- [51] KOHLES S.S., ROBERTS J.B., *Linear poroelastic cancellous bone anisotropy: trabecular solid elastic and fluid transport properties*, J. Biomech. Eng., 2002, 124, 521–526.
- [52] BAROUD G., FALK R., CROOKSHANK M., SPONAGEL S., STEFFEN T., *Experimental and theoretical investigation of directional permeability of human vertebral cancellous bone for cement infiltration*, J. Biomech., 2004, 37, 189–196.
- [53] BEAUDOIN A.J., MIHALKO W.M., KRAUSE W.R., *Finite element modelling of polymethylmethacrylate flow through cancellous bone*, J. Biomech., 1991, 24(2), 127–136.
- [54] LI G.P., BRONK J.T., AN K.N., KELLY P.J., *Permeability of cortical bone of canine tibiae*, Microvasc. Res., 1987, 34(3), 302–10.